Available online at www.sciencedirect.com
SCIENCE DIRECT®
Carbohydrate Research 338 (2003) 2135–2147
CARBOHYDRATE RESEARCH
www.elsevier.com/locate/carres

Atomic force microscopy of pea starch granules: granule architecture of wild-type parent, *r* and *rb* single mutants, and the *rrb* double mutant

Michael J. Ridout,[a] Mary L. Parker,[a] Cliff L. Hedley,[b] Tatiana Y. Bogracheva,[b] Victor J. Morris[a,*]

[a] *Institute of Food Research, Norwich Laboratory, Norwich Research Park, Colney, Norwich NR4 7UA, UK*
[b] *John Innes Centre, Norwich Research Park, Colney, Norwich NR4 7UH, UK*

Received 23 September 2002; received in revised form 27 May 2003; accepted 10 June 2003

Abstract

AFM studies have been made of the internal structure of pea starch granules. The data obtained provides support for the blocklet model of starch granule structure (Carbohydr. Polym. 32 (1997) 177–191). The granules consist of hard blocklets dispersed in a softer matrix material. High-resolution images have yielded new insights into the detailed structure of growth rings within the granules. The blocklet structure is continuous throughout the granule and the growth rings originate from localised defects in blocklet production distributed around the surface of spheroidal shells within the granules. A mutation at the *rb* locus did not lead to significant changes in granule architecture. However, a mutation at the *r* locus led to loss of growth rings and changed blocklet structure. For this mutant the blocklets were distributed within a harder matrix material. This novel composite arrangement was used to explain why the granules had internal fissures and also changes in gelatinisation behaviour. It is suggested that the matrix material is the amylose component of the granule and that both amylose and amylopectin are present within the *r* mutant starch granules in a partially-crystalline form. Intermediate changes in granule architecture have been observed for the double mutant *rrb*.
© 2003 Elsevier Ltd. All rights reserved.

Keywords: Starch granule structures; Growth rings; AFM; Atomic force microscopy; Near-isogenic pea starch mutants

1. Introduction

The prospect of being able to design starches for specific industrial uses, by genetic manipulation of the biosynthetic pathway, has led to renewed interest in the structure of starch granules and their bio-assembly.[1] Advances in the understanding of starch biosynthesis have benefited from the use of genetic variation and, in particular, the identification of specific mutations that affect defined steps in the biosynthetic pathway.[2] Genetics also provides a tool for investigating the architecture of starch granules, and for establishing links between the granule structure and the functional behaviour of the starch. Such studies require suitable genetic material and simple, reproducible methods for probing granule ultrastructure.

A range of mutants developed in peas provides a suitable vehicle for such studies: these mutants are known to be affected at specific steps in the starch biosynthetic pathway.[3–7] The mutants have been backcrossed into a common background and can now be considered as near-isogenic apart from those genes at the loci where mutations have been identified. All of the mutants produce starches that differ from the wild-type in the proportions of amylose and amylopectin.[8] Genes at three of the loci (*rb*, *rug3* and *rug4*) encode enzymes that determine the supply of substrate during biosynthesis: namely ADP glucose pyrophosphorylase, phosphoglucomutase and sucrose synthase, respectively.[2] The genes at the other three loci (*lam*, *rug5* and *r*) encode enzymes that involve direct synthesis of starch polysaccharides: these are respectively starch synthase I,

* Corresponding author. Tel.: +4-1603-255271; fax: +4-1603-507723.
E-mail address: vic.morris@bbsrc.ac.uk (V.J. Morris).

0008-6215/03/$ - see front matter © 2003 Elsevier Ltd. All rights reserved.
doi:10.1016/S0008-6215(03)00309-4

involved in amylose synthesis, and starch synthase II and starch branching enzyme A, which are considered to be involved in amylopectin biosynthesis.[2]

Wild-type pea starch[9,10] contains 35% amylose and is a C-type starch with a total crystallinity of 20%. The crystalline structure of pea starch granules has been shown to consist of both A and B polymorphs[9,10] with B polymorphs arranged centrally and the A polymorphs peripherally within each granule.[11,12] Mutations in genes that influence the flow of substrate during biosynthesis (*rb*, *rug3* and *rug5*) resulted in starches with changes in the total level of crystallinity and possibly increased the relative content of A polymorphs in the starches.[8] Genes affecting synthesis of starch polysaccharides (*r*, *rug5* and *lam*) had little effect on the total crystallinity but increased the content of B polymorphs, with the *r* mutant becoming purely B-type.[8] During gelatinisation, the *rb*, *rug3*, *rug4* and *lam* mutants retained narrow endothermic peaks similar to the behaviour of the wild-type, although each starch had different peak temperatures and enthalpy changes. By contrast, starches from *r* and *rug5* mutants were very different showing broad transitions during gelatinisation.[8] The *rrb* double mutant shows intermediate behaviour reflecting the different influences of the two genes.[13] In trying to relate these specific genetic mutations to changes in starch functionality, it is important to identify genetically-induced changes in the architecture of the starch granules.

The current view of starch granule structure is described in recent reviews.[14,15] The conventional model of starch consists of a semi-crystalline granular structure that is composed of concentric shells of 'amorphous' and 'crystalline' growth rings. Crystallinity is considered to arise from the branches of the amylopectin molecules. On the basis of tomographic reconstruction of transmission electron micrographs of treated sectioned potato starch granules, Oostergetal and Bruggen have proposed an extremely detailed model of granule structure.[16] This model has received support from recent X-ray microfocus diffraction data[17] and incorporation of the concept of the side-chain liquid crystalline model of starch.[18,19] A further model suggested by Gallant and coworkers introduces an additional level of structural organisation termed blocklets.[15] The blocklets are essentially pictured as parcels of crystals distributed within the growth rings. Support for this model has come from recent atomic force microscopy (AFM) studies of starch granule surfaces[20] and the internal structure of starch granules.[21] The blocklets may be the precursors of the 'amylopectin particles' recently observed during the gelatinisation of starch.[22,23] Observation of blocklets in native starch granules will require high-resolution methods such as AFM that do not spatially average the granule structure. AFM thus provides a suitable route for the investigation of the effects of genetic mutations on the ultrastructure of starch granules. However, AFM studies of the internal structure of starch granules require flat surfaces, best obtained by the preparation of sections of embedded granules.[21,24] Recent studies have shown that the choice of embedding resin can influence the contrast in the AFM images, and may introduce artifacts into the images.[24] A new methodology has been developed, using a non-penetrating resin, which allows routine imaging of the starch granule ultrastructure under near-native conditions.[24] This article describes the use of this method to investigate the ultrastructure of selected near-isogenic pea starch mutants.

2. Materials and methods

Pea starch was extracted from the seeds of the wild-type parental line and from a series of mutants that are near-isogenic to this wild-type except for genes at the *r* and *rb* loci. The method of extraction is based on the procedure described previously by Bogracheva and coworkers.[8,25] Pea seeds were ground in a Cyclotec 1093 sample pin-mill (Sweden) and the resulting meal was slurried in water at a solid–liquid ratio of 1 to 12, the pH being adjusted to 8.5 with 0.1 M NaOH. The mixture was centrifuged at 2500*g* and the supernatant then removed. The precipitate had a very viscous green top layer and a solid white main part. The green top layer was removed and the rest of the precipitate was re-suspended in distilled water. This centrifugation and separation procedure was repeated twice, until the viscous layer was no longer present. The resulting uniform white precipitate was then re-suspended in distilled water and screened sequentially through two sieves of mesh sizes 300 and 53 μm. The resulting starch was washed with water and air-dried.

The air-dried starch was mixed with rapid-set Araldite (Bostik Ltd) then transferred to a mould. Rapid-set Araldite sets in about 2 min and hardens within 24 h, after which time the sections could be cut. Sections, nominally 1.5 μm thick, were cut onto water with glass knives using an Ultramicrotome (Ultracut E, Reichert-Jung). The sections were immediately transferred to a drop of distilled water on a glass slide. Individual sections were swiftly moved from the edge of the drop to an area of dry glass and the slide left to dry at room temperature. Although it was possible to cut thinner or thicker sections, a thickness of about 1.5 μm maintained the integrity of the starch granules during sectioning and minimised starch swelling on contact with water.

For light microscopy, whole starch grains or sections were generally stained with very dilute iodine in potassium iodide and then the unstained or stained samples were examined and photographed in an Olympus BX60 microscope equipped with digital image acquisition software (Syncroscopy, Cambridge).

AFM studies were made using a Thermomicroscopes Lumina combined AFM/SNOM system. Sections were scanned in air using the 'dry-scanner attachment'. Samples were scanned in the dc contact mode and recorded as topographical and error signal mode images. SiN_3 cantilevers were used with a nominal force constant of 0.38 Nm^{-1}. Scan sizes ranged from about 100 μm down to about 1 μm. The scan rate was generally between 2.0 and 2.5 Hz. For the force modulation studies, the cantilevers were driven at a frequency of 5 kHz into the sample surface with amplitudes of 4.0 nm.

3. Results and discussion

Previous studies on rapid-set Araldite-embedded starches have shown that this technique provides reproducible images of the internal structure of near-native starch.[24] The embedding resin does not penetrate into the granule and thus the features observed within the boundaries of the granules are entirely due to the internal structure of the starch granule.[24] Typical low-resolution AFM images of wild-type pea starch are shown in Fig. 1. Light microscope images of iodine-stained sections are shown in Fig. 2(a). These images show sectioned granules of a range of size and shapes. Part of this variation will be due to the fact that not all the sections are cut through the centre of the granule. For those sections that are clearly cut through the centre of the granules, where the hilum is visible, the size and shapes observed are typical of pea starch.[11,26] In Fig. 1(a) there is a dark hole where a granule has fallen out of the section enabling the thickness of the section to be confirmed as 1.5 μm. The height variation across the sectioned granules (Fig. 1(a and c)) appears to result from folds around the edges of the granule. These are most likely artifacts that are known to occur when sections are cut onto water during the sectioning procedure.[21,27] We have observed similar effects for potato starch sections embedded in rapid-set Araldite.[24] The error signal mode images (Fig. 1d–f) show the growth rings most clearly. There is good agreement between the AFM images (Fig. 1d–f) and the light microscopy images (Fig. 2a). At the very centre of the granule (marked 'cen' in Fig. 1e) near the hilum there are no discernable growth rings. Further out from the centre of the granule growth rings can be seen. These AFM images of the granule have been obtained without iodine staining or any of the modifications, such as lintnerisation or enzyme digestion, normally used to enhance the contrast between the 'amorphous' and 'crystalline' regions within the granule. Near the centre of the granule, the spacing of the growth rings is about 800 nm and this reduces to about 300 nm towards the edges of the granules (Fig. 1(e)). This is consistent with the light microscopy images (Fig. 2(a)). At higher resolution, the internal surface of the granule has a rough, mottled appearance (Fig. 3). This is true for both the centre of the granule, where no growth rings are seen, and for regions within and between growth rings. These higher resolution images (Fig. 3) show features ranging in shape from circular to elliptical: such features being most easily seen in the error signal mode image (Fig. 3(b)). The most asymmetric structures have an axial ratio of 2:1 with a maximum length of about 130 nm. The size and shapes of these features seem to be the same at the centre of the granule and further out towards the edge of the granule. These images support the proposed blocklet model of starch structure.[15] High-resolution images spanning growth rings suggest that the growth rings, and the regions between them, contain loosely-assembled layers of blocklets. Also the so-called 'amorphous' growth rings (labeled a) are not continuous structures. Rather, in some regions (arrowed c) there is a continuous stream of blocklets from one 'crystalline' growth ring, through the 'amorphous' boundary and into the next outer 'crystalline' zone. In neighbouring sites on the 'amorphous' zones (arrowed d) there are darker regions that may correspond to imperfect or missing blocklets. It appears to be this collection of defects, assembled on what one must assume to be the surface of a shell within the granule, which together generate the 'amorphous' growth ring. Locally, the elliptical blocklets are aligned with each other and the net orientation is not completely radial. The simplest three-dimensional structure for the blocklets would be a prolate ellipsoid. Variations in size and shape may reflect genuine changes in axial ratio or could result from different locations of sectioning planes through the blocklet: at present it is not possible to distinguish between these two options.

Force modulation imaging generates contrast that depends on the relative stiffness of different regions of the sample. Harder regions should appear brighter in the images. Fig. 3(c) shows high-resolution force modulation images of the wild-type pea samples. The blocklet structures appear bright relative to a darker background. This is consistent with the idea of partially-crystalline amylopectin contained within the blocklets and with the amylose lying in the regions surrounding the blocklets.[15]

The AFM images of the *rb* mutant starch (Fig. 4) are qualitatively similar to those of the wild-type parent (Fig. 1). The low-resolution AFM images show good agreement with the light microscopy images of iodine-stained sections (Fig. 2(b)). Once again there is some slight folding of the structure at the edges of the granule, best seen in the topographic AFM images (Fig. 4(a and c)). The sizes and shapes of the granules are as expected for pea starch.[26] Growth rings can be seen in the topographic images (Fig. 4(a, c and e)) but are much

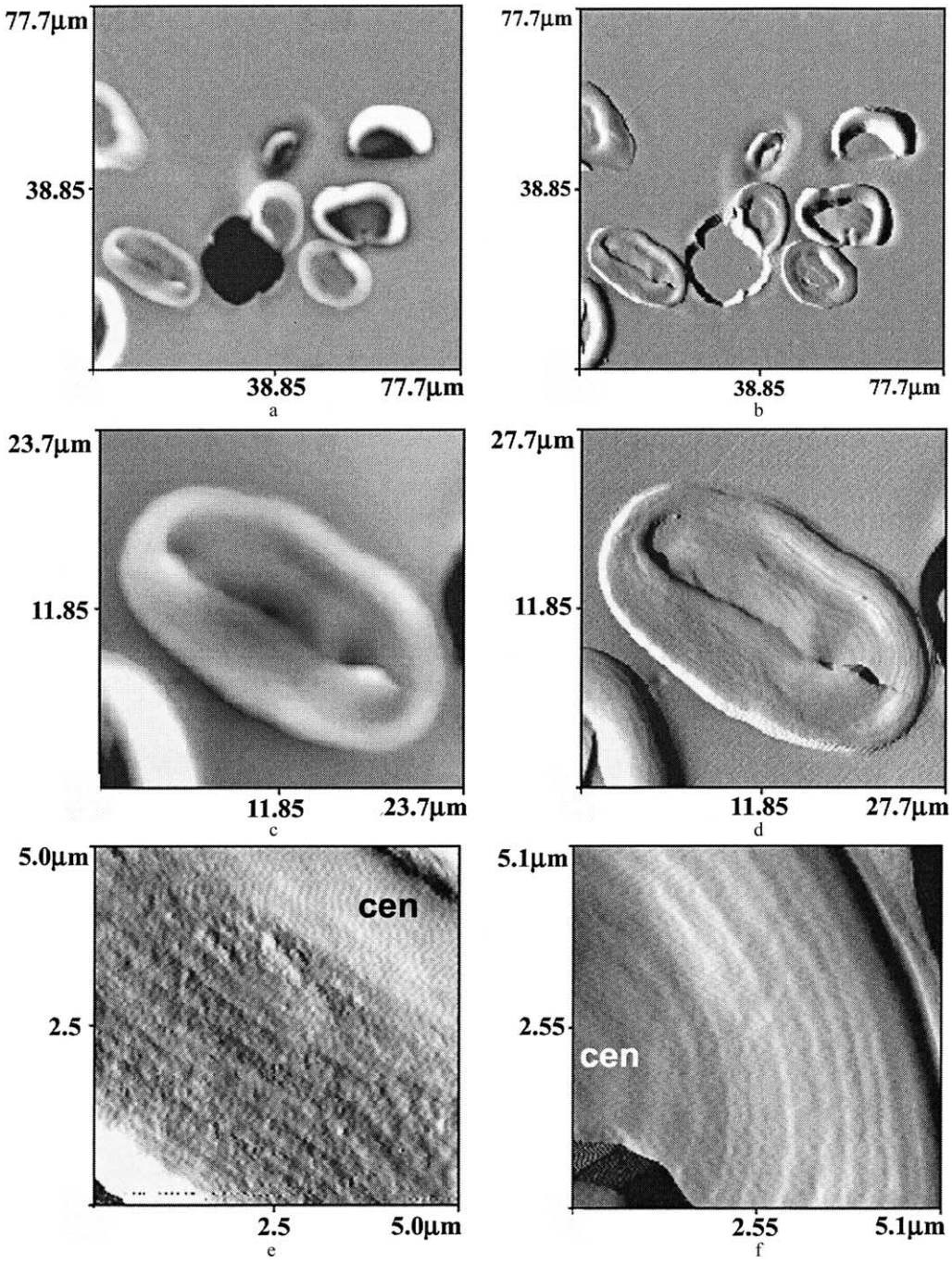

Fig. 1. Low- and medium-resolution AFM images of wild-type pea starch granules: (a and c) are topographic images; and (b, d, e and f) are error signal mode images. In (e and f) the central region of the granule within which no growth rings are seen is marked 'cen'.

clearer in the error signal mode images (Fig. 4(b, d and f)). The growth ring structure can be seen almost continuously throughout the granule, becoming closer together towards the outer edges of the granule, but the surfaces of the sections appear slightly rougher than the wild-type samples. The AFM images of unstained material correlate well with light microscopy of iodine-stained sections (Fig. 2(b)). Once again high-resolution AFM images (Fig. 5(a and b)) show discontinuous 'amorphous' growth rings (labeled a) with the blocklet size and shape similar within and between 'crystalline' growth rings. The higher resolution error signal mode images (Fig. 5(b)) show features ranging in shape from circular to elliptical. The most asymmetric structures have an axial ratio of 2:1 with a maximum length of about 150 nm.

Force modulation images of the *rb* mutant (Fig. 5(c)) are again similar to those seen for the wild-type starch

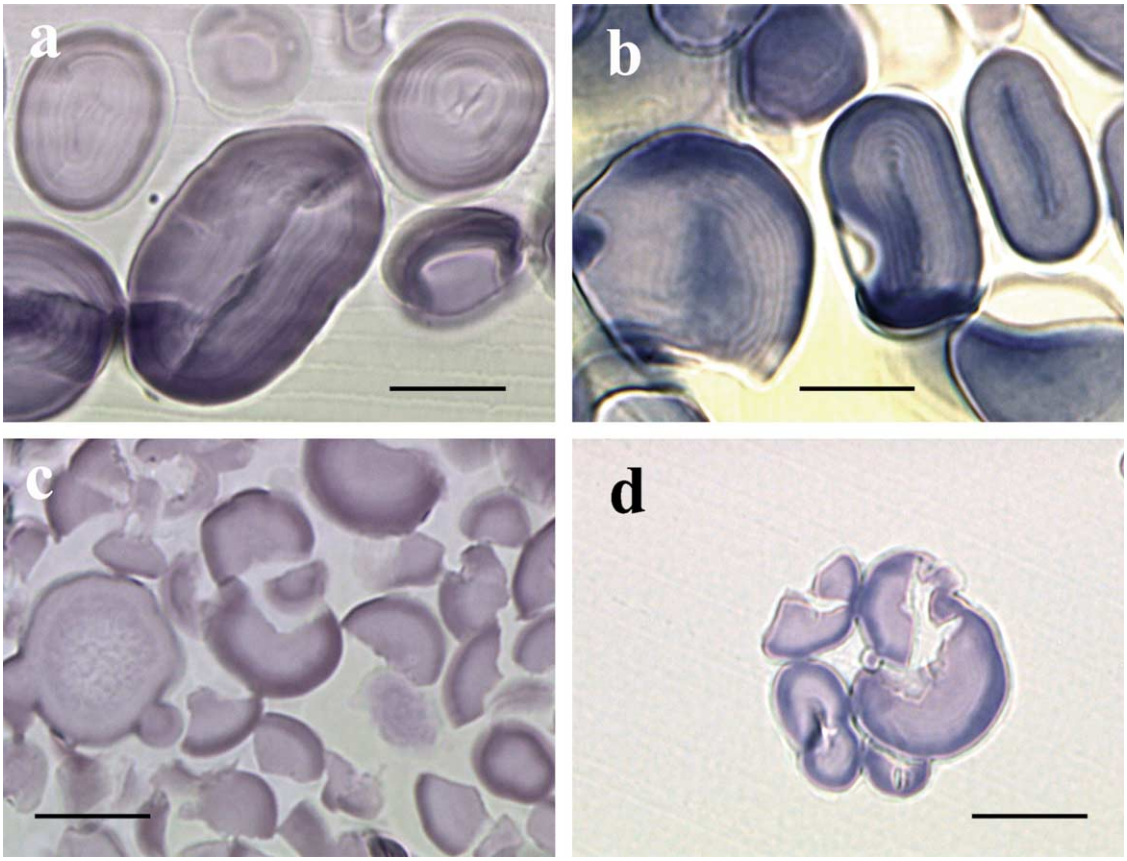

Fig. 2. Light microscopy of iodine-stained sections: (a) wild-type pea starch; (b) *rb* mutant; (c) *r* mutant; and (d) *rrb* mutant. Scale bar is 10 μm.

(Fig. 3(c)). The blocklet structures appear bright, consistent with crystalline amylopectin-based blocklets embedded in a softer amylose matrix.

By contrast, AFM images (Figs. 6, 8 and 9) of the *r* mutant show substantial differences to those of the wild-type samples (Figs. 1 and 3). Low-resolution topographic (Fig. 6(a and c)) and error signal mode images (Fig. 6(b and d)) show sharp irregular-shaped objects. Closer inspection reveals that these are fissured starch granules. In some samples the fissuring is incomplete and the different fragments remain partially attached to each other. This is borne out by light microscopy images of whole grains (Fig. 7) and sectioned material (Fig. 2(c)). The light micrographs show representative types of structure. There are a few near-spherical granules showing a central region with different contrast (marked

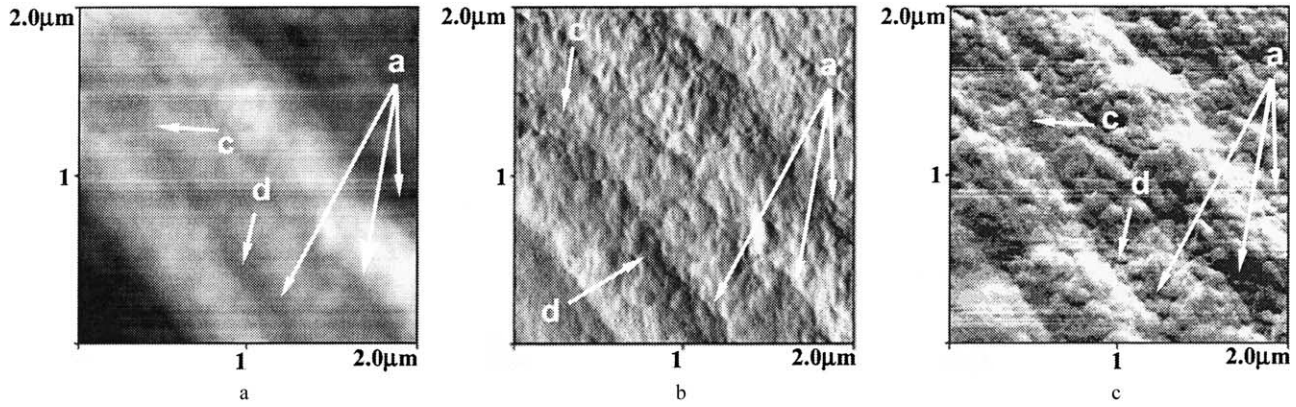

Fig. 3. High-resolution AFM images of wild-type pea starch granules: (a) topography image; (b) error signal mode image; and (c) force modulation image. The 'amorphous' growth rings are marked 'a', the regions where blocklets pass continuously across these 'amorphous zones' are marked 'c', and the defect regions are marked 'd'.

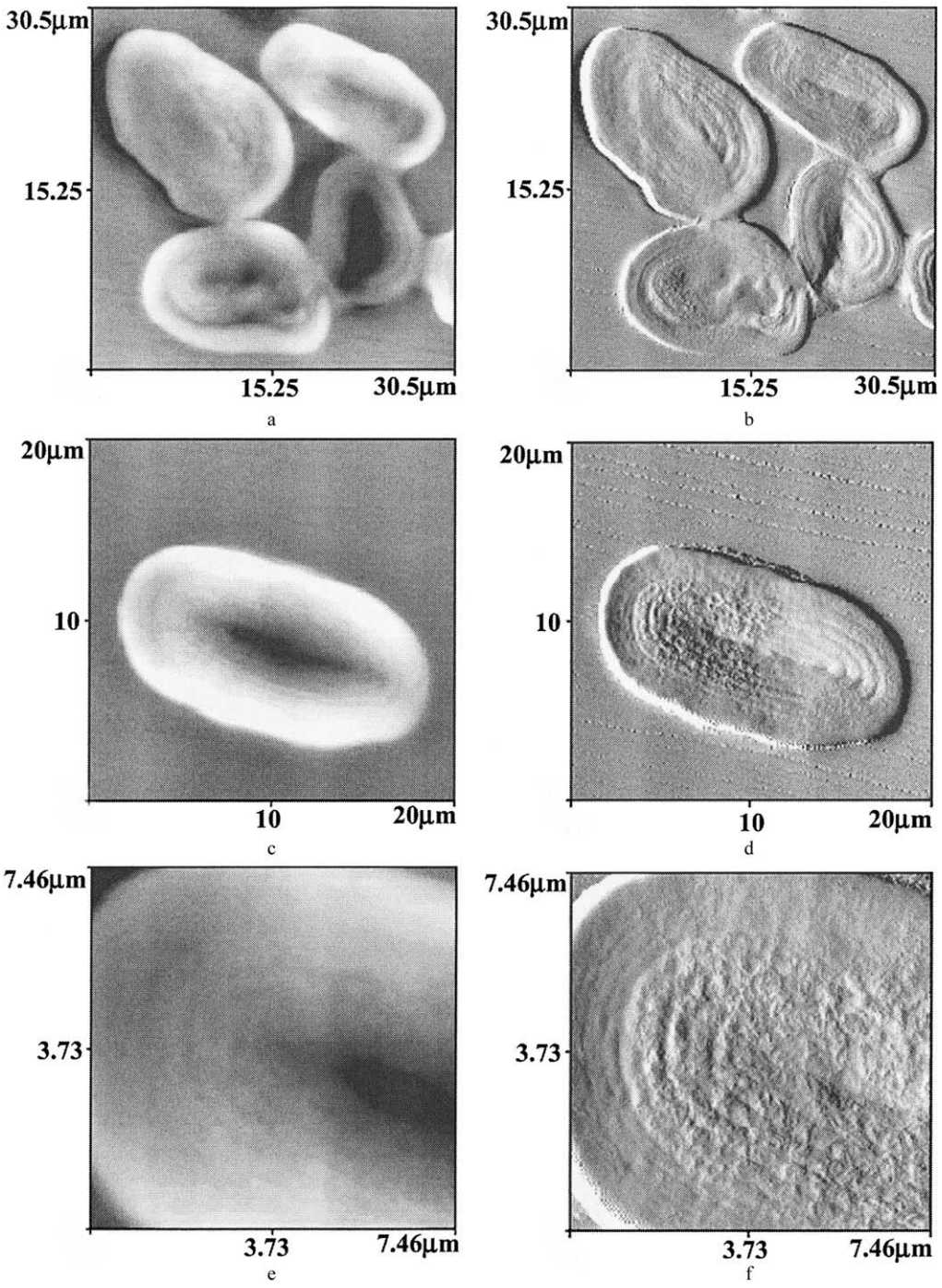

Fig. 4. Low- and medium-resolution AFM images of *rb* mutant pea starch granules: a, c and e are topographic images and b, d and f are error signal mode images.

'a' in Fig. 7). A significant fraction of the granules are of the type marked 'b' in Fig. 7, showing internal fissures radiating out from the centre of the granule. The remaining material is in the form of partially-disrupted granules or granule fragments (Fig. 2(c), Fig. 6 and the insert in Fig. 7). Thus the images appear to indicate fissuring and progressive fragmentation of the starch granules. Comparison of the light microscopy images of whole grains and sectioned material confirms that the fissuring and fragmentation of the granules is not an artifact of the embedding and sectioning process. The topographical AFM images (Fig. 6(a and c)) show flat samples with less evidence of folding at the edges of the granules than that seen for the wild-type parent (Fig. 1). Even in the error signal mode images (Fig. 6(b and d)) there is no evidence for any growth ring structure

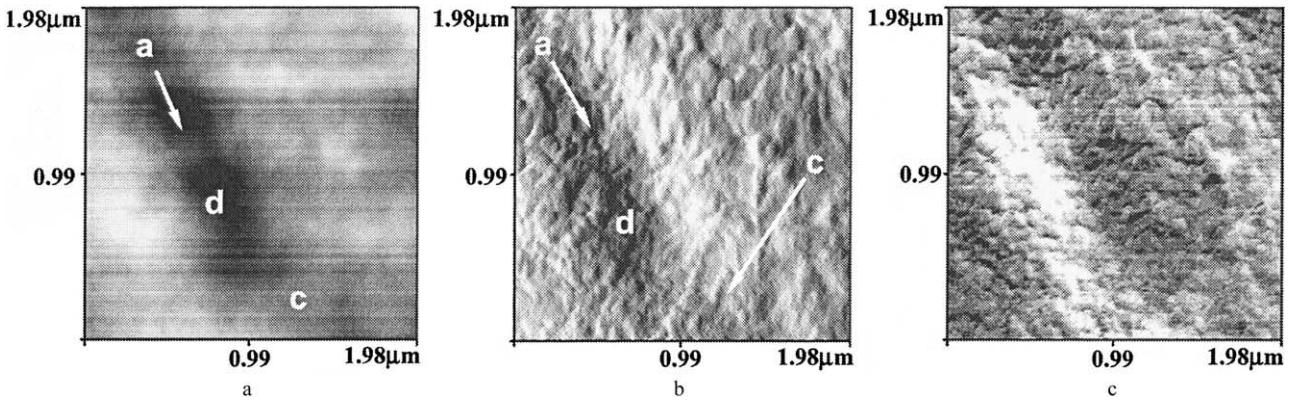

Fig. 5. High-resolution AFM images of *rb* mutant pea starch granules: (a) topography image; (b) error signal mode image; and (c) force modulation image. The 'amorphous' growth rings are marked 'a', the regions where blocklets pass continuously across these 'amorphous zones' are marked 'c', and the defect regions are marked 'd'.

throughout the granule. Similarly no growth ring structures are apparent in light micrographs of the iodine-stained sectioned material (Fig. 2(c)). However, even at relatively low-resolution the AFM images reveal a granularity of the section surface (Fig. 6(d)). At higher resolution (Fig. 8) even in the topographic images (Fig.

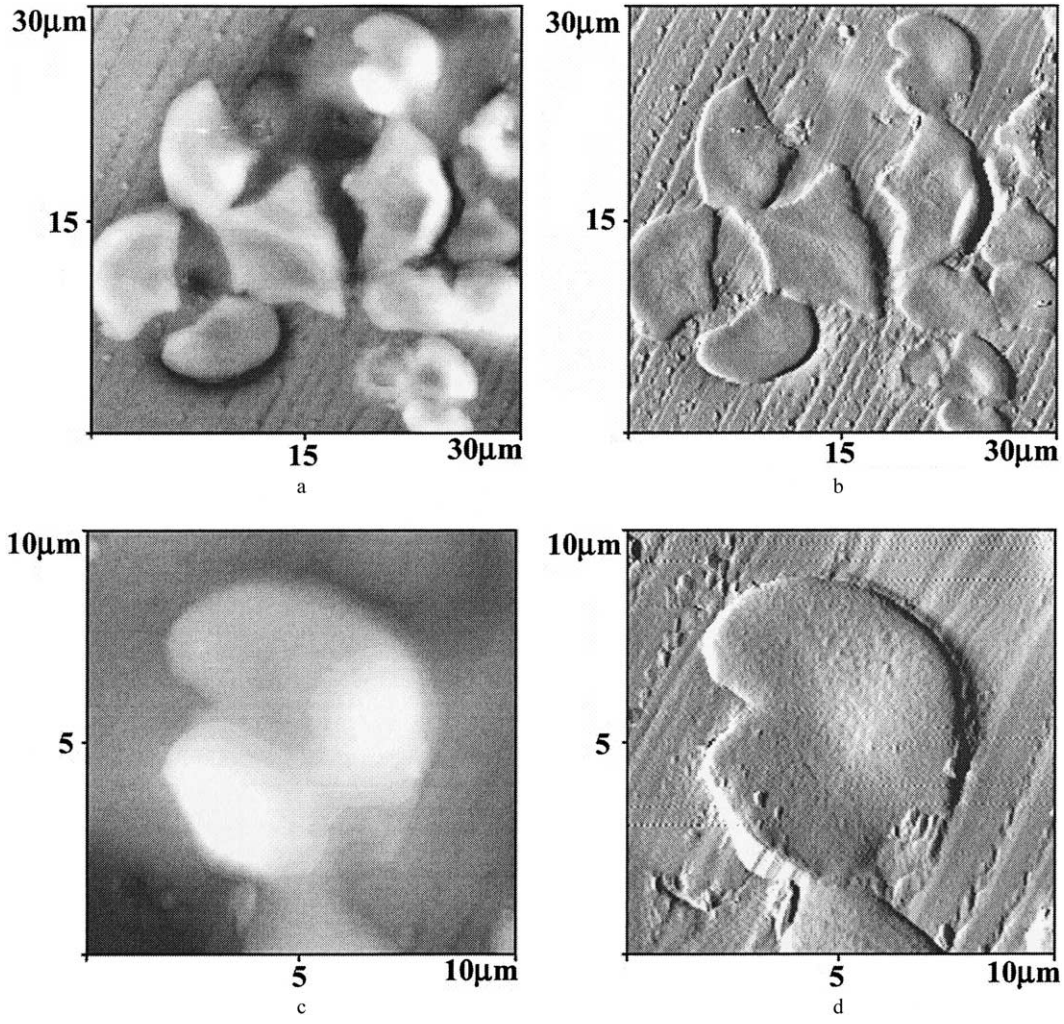

Fig. 6. Low- and medium-resolution AFM images of *r* mutant pea starch granules: a and c are topographic images and b and d are error signal mode images.

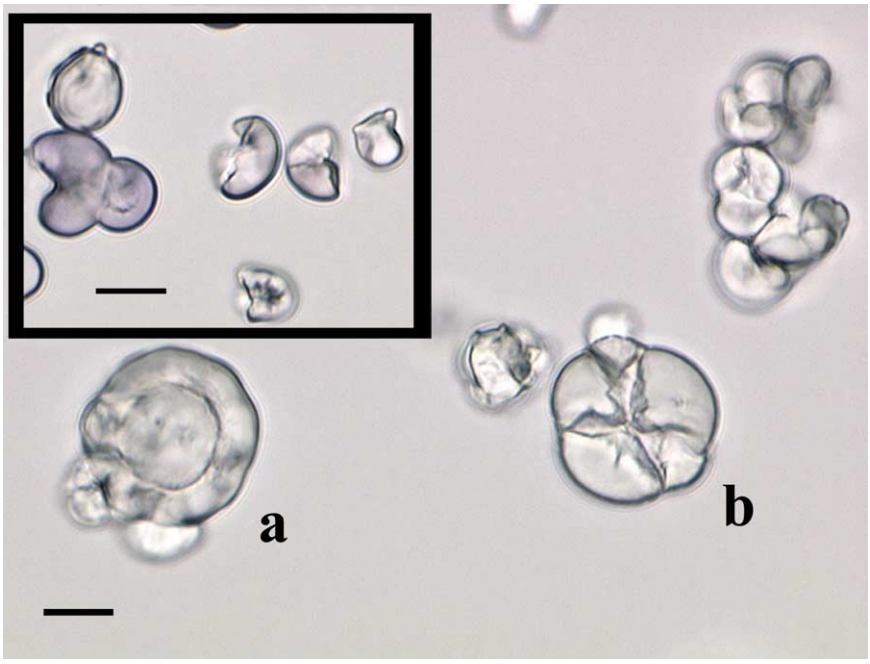

Fig. 7. Light microscopy of *r* mutant pea starch grains. Scale bar is 10 μm. Examples are shown of unstained granules marked 'a' showing distinct inner regions, unstained granules marked 'b' showing radial fissures and an insert showing intact iodine-stained broken granules and granule fragments.

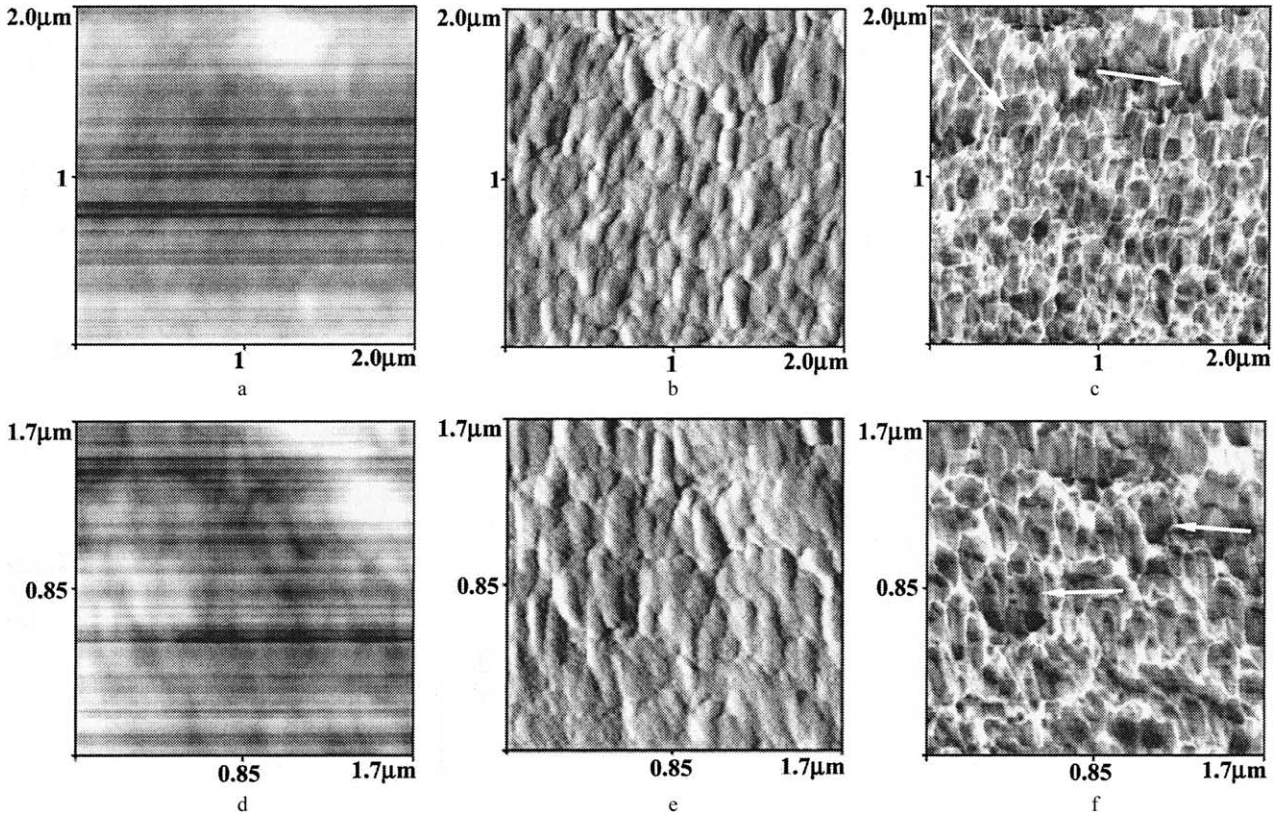

Fig. 8. High-resolution AFM images of *r* mutant pea starch granules: (a and d) are topographic images; (b and e) are error signal mode images; and (d and f) are force modulation images. The arrows in c and f indicate bright interconnecting matrix surrounding groups of blocklets.

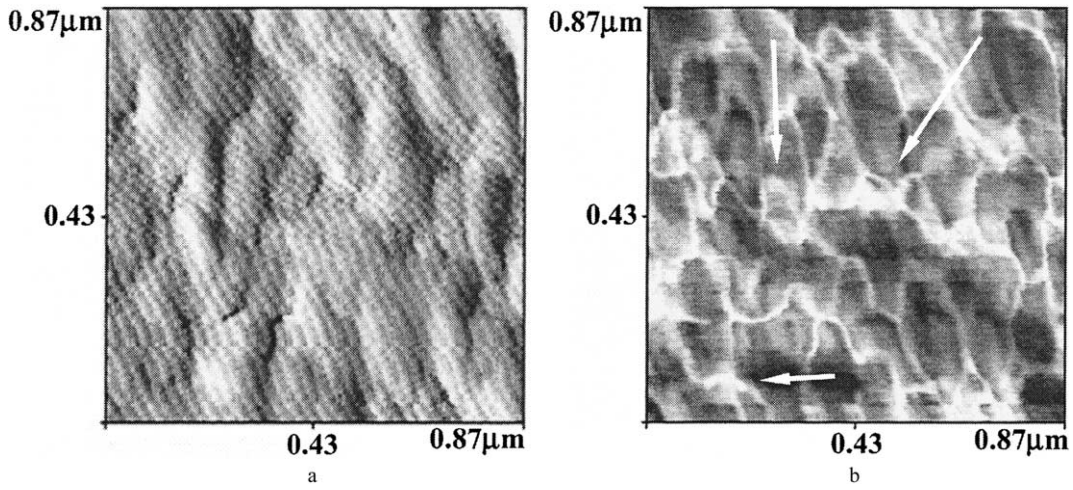

Fig. 9. Higher-resolution AFM images of *r* mutant pea starch granules: (a) is an error signal mode image; and (b) is a force modulation image. The arrows in b indicate regions where the bright interconnecting matrix passes through a blocklet.

8(a and d)), but particularly in the error signal mode images (Fig. 8(b and e), Fig. 9(a)), objects attributable to blocklet structures can be seen. These show a range of sizes and shapes, with elliptical structures of axial ratios up to 3:1 and major dimensions up to 250 nm in length. Clearly this mutation leads to substantial changes in granule architecture.

Force modulation images highlight harder, stiffer regions within the granule. The force modulation images of the *r* mutant (Fig. 8(c and f), Fig. 9(b)) are strikingly different from those of the wild-type (Fig. 3(c)) and *rb* mutant (Fig. 5(c)). In this instance, the brightest regions within the image are the interconnecting matrix within which the blocklets are enclosed. Close comparison of the force modulation and error signal mode images in Figs. 8 and 9 reveals that, although the majority of the interconnecting network is bright, there are regions where blocklets are grouped together and the grouping is encompassed by a bright boundary, rather than a bright boundary enclosing each individual blocklet. Such features are arrowed in Fig. 8(c and f). There are also regions where bright bands are seen to cross blocklet structures and such examples are highlighted by arrows in Fig. 9(b). The brightness of the boundary regions suggests that the interconnecting matrix is now stiffer than the blocklet structures. The wild-type parent and the two mutants (*r* and *rb*) can be considered as composite structures. For the wild-type parent and the *rb* mutant the softer matrix can accommodate small expansions or contractions of the granule, preventing fracture of the blocklets. However, for the *r* mutant the harder matrix material may not be able to accommodate such changes and this could offer an explanation for the fissured granules seen in Fig. 2(c), Figs. 6 and 7. Slight expansions or contractions of the granules, probably during seed maturation or maybe on extraction, due possibly to small changes in water content, would stress the stiff network causing it to fail at the weakest points and thus relieve the stress within the granule. This would explain the fissures and subsequent breakdown of the granule structure.

In order to explain the enhanced hardness of the matrix material, it is tempting to suggest that in the *r* mutant, the generation of excess amylose (up from 35 to 65%)[8] leads to crystallisation of a fraction of this material forming the hard matrix. Some support for this suggestion comes from lintnerisation studies of the granules.[8] For the *r* mutant, the profile of amylosic chains contained within the crystalline regions is very broad,[8] and much broader than the branch length distribution of the amylopectin, which remains fairly similar to that of the wild-type amylopectin.[28] The formation of a crystalline amylose matrix would affect the gelatinisation of the starch. The melting point of amylosic crystals depends on chain length[29] and this could account for the broadened gelatinisation behaviour seen for the *r* mutant. The presence of an interconnected crystalline matrix (physical cross linking) would inhibit swelling of the granule until the crystal structure melts at sufficiently high temperatures. This effect could be likened to cross-linking in a chemically-modified starch. If the above picture is correct, it lends credence to the idea that amylose and amylopectin are largely compartmentalised within the granule.

Figs. 10 and 11 shows AFM images of the double mutant *rrb*. At low-resolution the samples are similar to those of the *r* mutant (Fig. 6) showing fragmented granules with sharp fracture planes. Fragmentation of the granules is also apparent from the light microscopy images of unstained granules (Fig. 12) and sectioned iodine-stained material (Fig. 2(d)). The AFM images of the sections are quite flat with little evidence in the topographic images (Fig. 10(a and c)) for folding at the edges of the granules. Unlike the *r* mutant, but like the

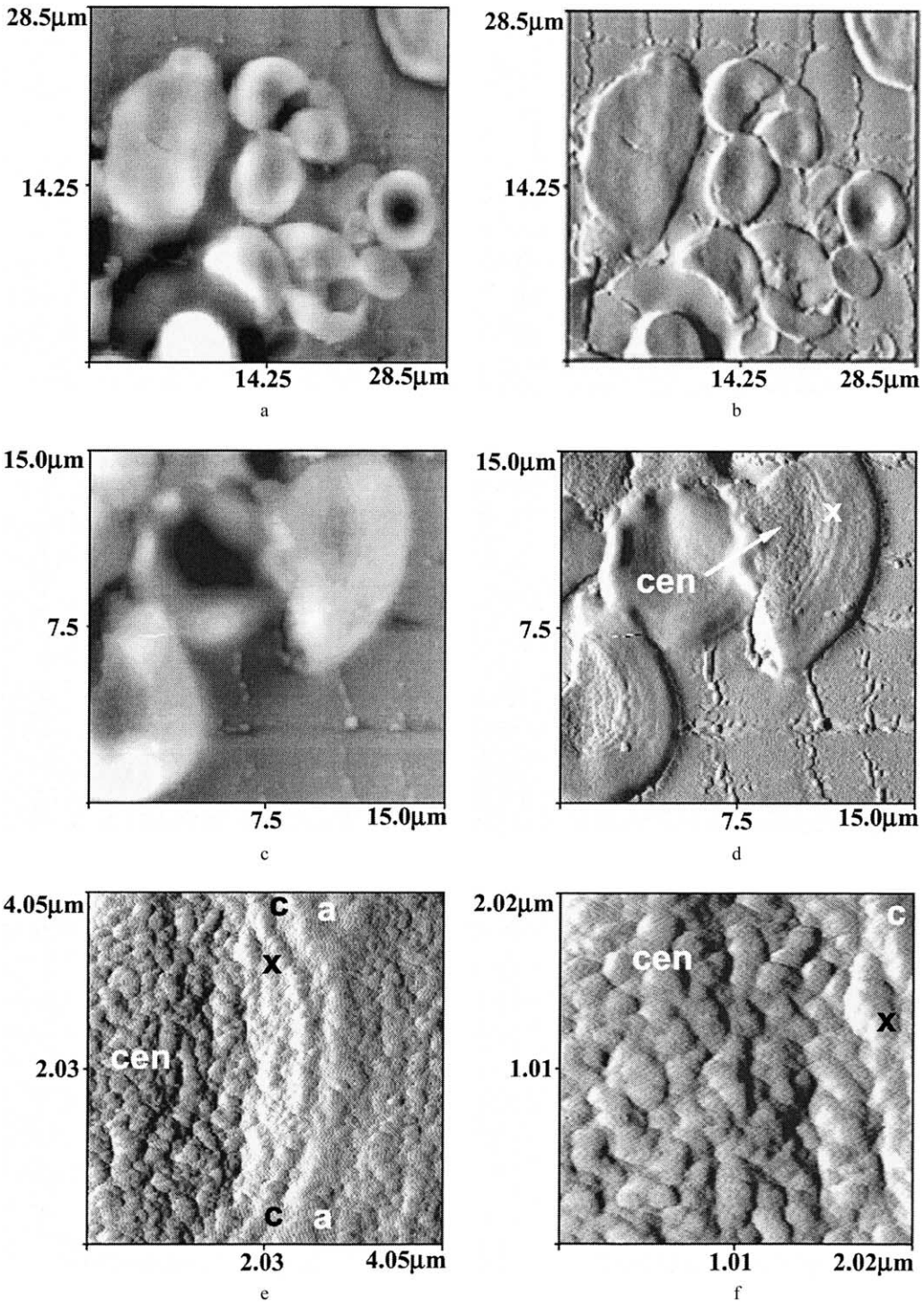

Fig. 10. AFM images of *rrb* double mutant pea starch granules: (a and c) are topographic images; and (b, d, e and f) are error signal mode images. The central region of the granule within which no growth rings are seen is marked 'cen' in (d, e and f). The position X in the fragmented granule shown in d is indicated in (e and f). 'Amorphous' and 'crystalline' growth rings are marked 'a' and 'c' in e and f.

rb mutant, the granules show discernable growth rings. These are most clearly seen in the error signal mode images (Fig. 10(d–f)). The growth ring structure is very clearly defined in the AFM images but difficult to detect in the light microscopy of the iodine-stained sectioned material (Fig. 2(d)). The AFM data shows that there is a small central region ('cen' arrowed in Fig. 10(d)) in which no growth ring structure is visible. Outside this central region, growth rings become closer together towards the edges of the granule (Fig. 10(d)). At higher

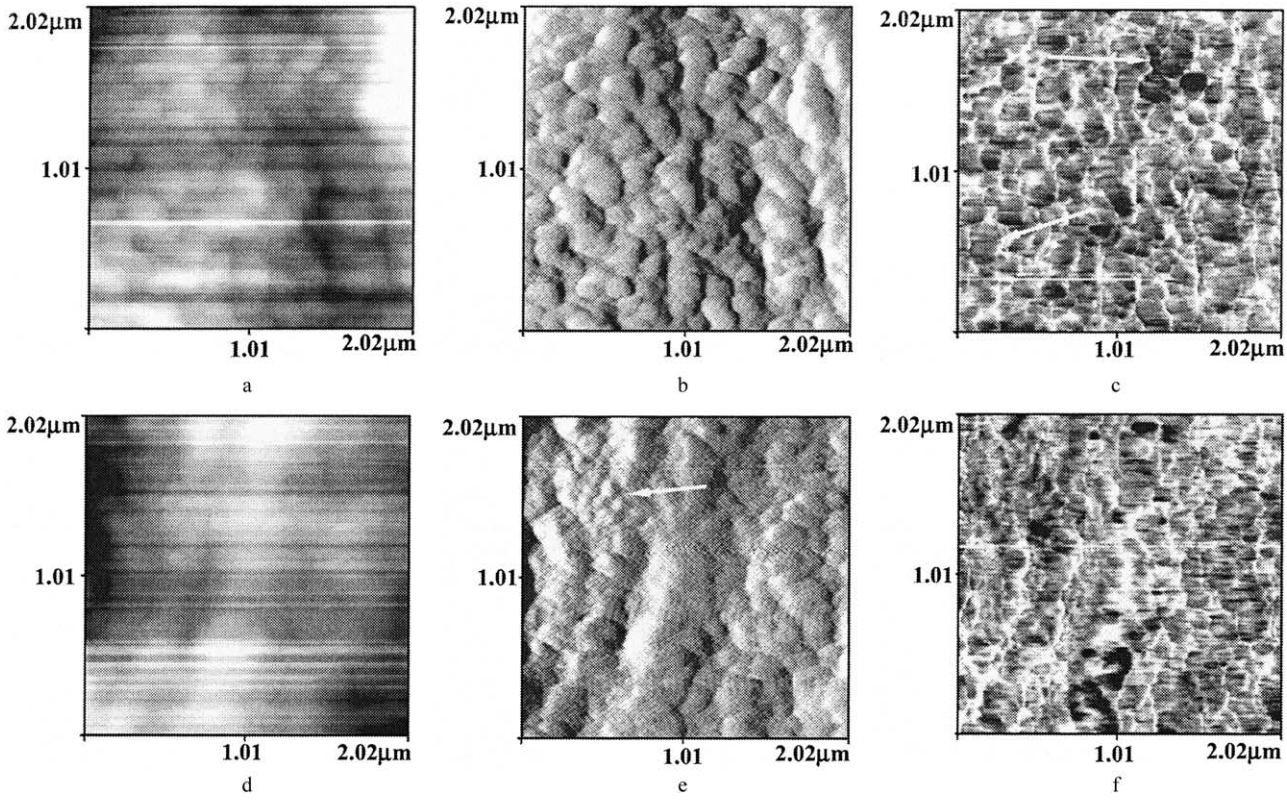

Fig. 11. High-resolution AFM images of *rrb* double mutant pea starch granules: (a and d) are topographic images; (b and e) are error signal mode images; and (c and f) are force modulation images. The arrowed region in c indicates bright interconnecting matrix material enclosing a group of blocklets.

resolution, features taken to be blocklets can be seen within the central region (marked 'cen' in Fig. 10(e)), and within both the 'amorphous' and 'crystalline' growth rings (marked a and c in Fig. 10(e)). Generally the size and shape of the blocklets seems to be similar at all points within the granule: the blocklets are circular

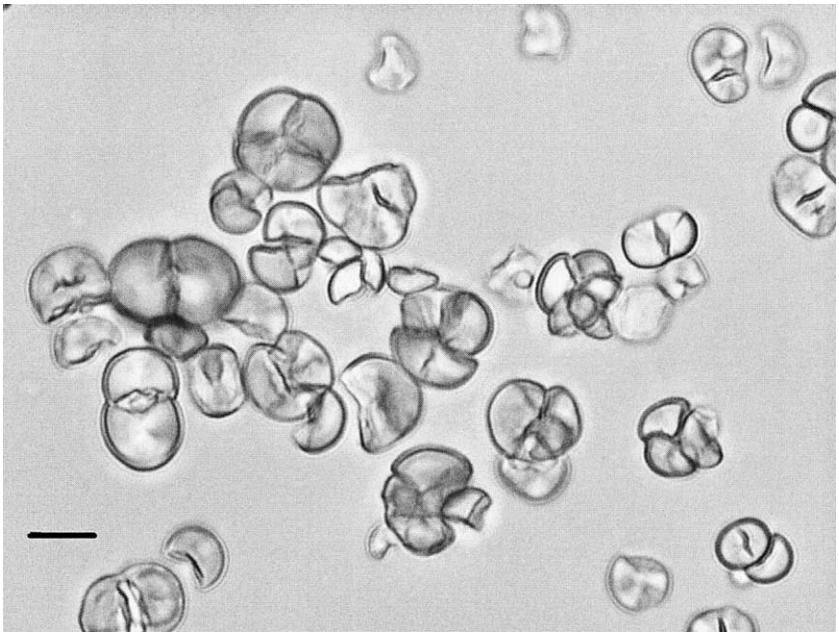

Fig. 12. Light microscopy of unstained *rrb* pea starch granules. Scale bar is 10 µm. The field of view shows granules with radial fissures, broken granules and granular fragments.

suggesting a spherical shape with a diameter of 126 nm. At a few regions within granules, group of smaller blocklets similar in size to those of the wild-type parent, are observed and an example of this is arrowed in Fig. 11(e).

The force modulation images of the double mutant *rrb* (Fig. 11(c and f)) resemble those of the *r* mutant (Fig. 8(c and f), Fig. 9(b)). The interconnecting matrix appears bright relative to the blocklets. This would suggest that this matrix region is stiffer and possibly more crystalline than the blocklets. This would be consistent with the observed tendency for internal fissures within the granules. As with the *r* mutant there are regions (arrowed in Fig. 11(c)) where the brighter matrix surrounds groups rather individual blocklets.

4. Conclusions

Novel AFM images have been obtained of the internal structure of starch granules of wild-type pea starch and the near-isogenic *r*, *rb* and *rrb* mutants. The high-resolution images obtained support the blocklet model[15] of starch granule architecture. For the wild-type and *rb* mutants, the force modulation images support the idea of stiffer blocklets suspended in a softer matrix. The high-resolution AFM images suggest a totally new interpretation of the internal structure of the starch granule. These images imply that the blocklet structure is continuous throughout the granule and the so-called 'amorphous' growth rings in the native granule are composed of a collection of localised defects in blocklet structure, distributed around the surface of shells within the granule.

The present data suggest the need to refine the 'blocklet model' of starch granule structure introduced by Gallant and coworkers.[15] The AFM images imply that the blocklet structure is uniform throughout the granule and that the blocklets are embedded in a softer matrix material. This structured nature of the granule is interrupted by localised defects in blocklet production that appear to be distributed on the surfaces of spheroidal shells within the granule. It is suggested that these defect regions are the origins of the growth ring structures seen in modified or stained granules. Following Gallant and coworkers[15] it might be considered that the blocklets correspond to partially-crystalline amylopectin and that amylose is predominately distributed within the softer matrix material.

The *r* mutation causes striking changes in the architecture of the granule, resulting in the loss of growth rings and an altered blocklet structure. The most noticeable change in granule architecture has been revealed by force modulation AFM studies. These measurements imply that, in the *r* mutant, the interconnecting matrix within which the blocklets are distributed is stiffer than the blocklets. It has been tentatively suggested that this could be attributed to crystallisation of amylose within the granule. It is proposed that the presence of this harder matrix structure accounts for the observed fissuring of the granules and the changes in gelatinisation behaviour. These studies also provide evidence taken to favour compartmentalisation of amylose and amylopectin within the granules. The double mutant *rrb* is observed to show intermediate behaviour between that observed for the *r* and *rb* single mutants.

Acknowledgements

The research described in this article was supported in part by the BBSRC core grant funding to the JIC and IFR and through funding from the EU Framework 4 FAIR (CT98-3527) programme. Apparatus used for the AFM studies was purchased through the award of a BBSRC Bioimaging grant, D11154. The authors wish to acknowledge useful discussions with Patrick Gunning and Steve Ring.

References

1. Heyer, A. G.; Lloyd, J. R.; Kossmann, J. *Curr. Opin. Biotechnol.* **1999**, *10*, 169–174.
2. Wang, T. L.; Bogracheva, T. Ya.; Hedley, C. L. *J. Exp. Botany* **1998**, *49*, 481–502.
3. Harrison, C. J.; Hedley, C. L.; Wang, T. L. *Plant J.* **1998**, *13*, 753–762.
4. Hylton, C.; Smith, A. M. *Plant Physiol.* **1992**, *99*, 1626–1634.
5. Wang, T. L.; Barber, R. A.; Denyer, K.; Hedley, C. L.; Hylton, C. M.; Johnson, S.; Jones, D. A.; Marshall, J.; Smith, A. M.; Tatge, H.; Tomlinson, K. L. *Pisum Genetics* **1992**, *26*, 39–40.
6. Hedley, C. L.; Bogracheva, T. Ya.; Lloyd, J. R.; Wang, T. L., Manipulation of starch composition and quality in peas, in: G. R. Fenwick, C. L. Hedley, R. L. Richardson, S. Khoklhar (Eds.), Agri-Food Quality 95. An interdisciplinary approach, Royal Society of Chemistry, Cambridge; 1996, pp. 138–148.
7. Denyer, K.; Barber, L. R.; Burton, R.; Hedley, C. L.; Hylton, C. M.; Johnson, S.; Jones, D. A.; Marshall, J.; Smith, A. M.; Tatge, H.; Tomlinson, K.; Wang, T. L. *Plant Cell Environ.* **1995**, *18*, 1019–1026.
8. Bogracheva, T. Ya.; Cairns, P.; Noel, T. R.; Hulleman, S.; Wang, T. L.; Morris, V. J.; Ring, S. G.; Hedley, C. L. *Carbohydr. Polym.* **1999**, *39*, 303–314.
9. Gernat, Ch.; Radosta, S.; Damaschun, G.; Schierbaum, F. *Starch/Stärke* **1990**, *42*, 175–178.
10. Cairns, P.; Bogracheva, T. Ya.; Ring, S. G.; Hedley, C. L.; Morris, V. J. *Carbohydr. Polym.* **1997**, *32*, 275–282.
11. Bogracheva, T. Ya.; Morris, V. J.; Ring, S. G.; Hedley, C. L. *Biopolymers* **1998**, *45*, 323–332.

12. Buleon, A.; Gerard, C.; Riekel, C.; Vuong, R.; Chanzy, H. *Macromolecules* **1998**, *31*, 6605–6610.
13. Bogracheva, T. Ya.; Davydova, N. I.; Genin, Ya. V.; Hedley, C. L. *J. Exper. Bot.* **1995**, *46*, 1905–1913.
14. Buleon, A.; Colonna, P.; Planchot, V.; Ball, S. *Internat. J. Biol. Macromolecules* **1998**, *23*, 85–112.
15. Gallant, D. J.; Bouchet, B.; Baldwin, P. M. *Carbohydr. Polym.* **1997**, *32*, 177–191.
16. Oostergetel, G. T.; Bruggen, E. F. G. *Carbohydr. Polym.* **1993**, *21*, 7–12.
17. Waigh, T. A.; Hopkinson, I.; Donald, A. M.; Butler, M. F.; Heidelbach, F.; Riekel, C. *Macromolecules* **1997**, *30*, 3813–3820.
18. Waigh, T. A.; Perry, P.; Reikel, C.; Gidley, M. J.; Donald, A. M. *Macromolecules* **1998**, *31*, 7980–7984.
19. Waigh, T. A.; Kato, K. L.; Donald, A. M.; Gidley, M. J.; Reikel, M. J. *Starch/Stärke* **2000**, *52*, 450–460.
20. Baldwin, P. M.; Adler, A. J.; Davies, M. C.; Melia, C. D. *J. Cereal Sci.* **1998**, *27*, 255–256.
21. Baker, A. A.; Miles, M. J.; Helbert, W. *Carbohydr. Res.* **2001**, *330*, 249–256.
22. Atkins, N. J.; Abeysekera, R. M.; Cheng, S. L.; Robards, A. W. *Carbohydr. Polym.* **1998**, *36*, 173–192.
23. Atkins, N. J.; Abeysekera, R. M.; Robards, A. W. *Carbohydr. Polym.* **1998**, *36*, 193–204.
24. Ridout, M. J.; Gunning, A. P.; Wilson, R. H.; Parker, M. L.; Morris, V. J. *Carbohydr. Polym.* **2002**, *50*, 123–132.
25. Bogracheva, T. Y.; Wang, Y. L.; Wang, T. L.; Hedley, C. L. *Biopolymers* **2002**, *64*, 268–281.
26. Hedley, C. L.; Bogracheva, T. Ya.; Wang, T. L. *Starch/Stärke* **2002**, *54*, 235–242.
27. Gallant, D. J.; Guilbot, A. *Starch/Stärke* **1971**, *23*, 244–250.
28. Lloyd, J. R.; Hedley, C. L.; Bull, V. J.; Ring, S. G. *Carbohydr. Polym.* **1996**, *29*, 45–49.
29. Moates, G. K.; Noel, T. R.; Parker, R.; Ring, S. G. *Carbohydr. Res* **1997**, *298*, 327–333.